

Femtosecond-laser-written Ho:KGd(WO₄)₂ waveguide laser at 2.1 μm

ESROM KIFLE,¹ PAVEL LOIKO,² CAROLINA ROMERO,³ JAVIER RODRÍGUEZ VÁZQUEZ DE ALDANA,³ AIRÁN RÓDENAS,^{1,4} VIKTOR ZAKHAROV,² ANDREY VENIAMINOV,² MAGDALENA AGUILÓ,¹ FRANCESC DÍAZ,¹ UWE GRIEBNER,⁵ VALENTIN PETROV,⁵ AND XAVIER MATEOS^{1,*}

¹Universitat Rovira i Virgili, Departament Química Física i Inorgànica, Física i Cristal·lografia de Materials i Nanomaterials (FiCMA-FiCNA)-EMaS, Campus Sescelades, E-43007, Tarragona, Spain

²ITMO University, 49 Kronverkskiy Pr., 197101 St. Petersburg, Russia

³Aplicaciones del Láser y Fotónica, University of Salamanca, 37008 Salamanca, Spain

⁴Istituto di Fotonica e Nanotecnologie, Consiglio Nazionale delle Ricerche (IFN-CNR), Piazza Leonardo da Vinci 32, 20133 Milano, Italy

⁵Max Born Institute for Nonlinear Optics and Short Pulse Spectroscopy, Max-Born-Str. 2a, D-12489 Berlin, Germany

*Corresponding author: xavier.mateos@urv.cat

Received XX Month XXXX; revised XX Month, XXXX; accepted XX Month XXXX; posted XX Month XXXX (Doc. ID XXXXX); published XX Month XXXX

We report on efficient laser operation of the first holmium monoclinic double tungstate waveguide laser fabricated by femtosecond direct laser writing. A depressed-index buried channel waveguide with a 60 μm diameter circular cladding was inscribed in 5 at.% Ho³⁺:KGd(WO₄)₂. It was characterized by confocal microscopy, μ-Raman and μ-luminescence spectroscopy indicating well-preserved crystallinity of its core. Pumped by a thulium bulk laser, the holmium waveguide laser generated 212 mW at 2055 nm with a slope efficiency of 67.2%. The waveguide propagation losses were 0.94±0.2 dB/cm.

<http://dx.doi.org/10.1364/OL.99.099999>

Femtosecond direct laser writing (fs-DLW) is a powerful method to fabricate three-dimensional (3D) passive and active photonic microstructures of various geometries in transparent dielectric materials (glasses, ceramics and crystals) [1,2]. These materials absorb the energy of the fs pulses through nonlinear processes in a short time leading to an almost negligible heat transfer. This causes permanent modification of the material structure on the μm-scale leading to a change of the refractive index that can be positive or negative [2]. Fs-DLW has been found to be very suitable for the fabrication of optical waveguides (WGs). Compared to other known methods for WG fabrication (e.g., liquid phase epitaxy, pulsed laser deposition, etc.), fs-DLW offers short fabrication time, wide range of WG geometries and a large number of suitable materials, including low-symmetry crystals. In the latter case, fs-

DLW allows to preserve the advantageous anisotropic spectroscopic properties of the WG core region.

Fs-DLW WG lasers emitting in the spectral range of ~1 μm (based on Yb³⁺ and Nd³⁺ ions) have been well-studied in the past [3-5]. Less attention has been paid to the eye-safe ~2 μm range where the laser emission is achieved using Tm³⁺ or Ho³⁺ ions [6]. For the Ho³⁺ ion, the emission typically occurs slightly above 2 μm due to the ⁵I₇ → ⁵I₈ transition. Such emission spectrally overlaps with the absorption bands of H₂O and CO₂ molecules which are of interest for bio- and environmental sensing. The 2-μm emission can also be applied for further conversion to the mid-IR. Ho³⁺ ions can be pumped directly in the upper laser level (⁵I₇) leading to a very high slope efficiency approaching the Stokes limit [7].

To date, only few studies have been reported dedicated to the fs-DLW Ho WG lasers. In [8], a Tm³⁺,Ho³⁺-codoped ZBLAN glass WG laser pumped by a Ti:Sapphire laser generated 76 mW at 2052 nm with a slope efficiency η of 20% (vs. the absorbed pump power). A singly Ho³⁺ doped ZBLAN glass WG laser in-band pumped by a Tm fiber laser was scaled to 1.09 W at 2070 nm with η = 50.9% (vs. the incident pump power) [9]. Its emission spectrum was also continuously tuned from 2004 to 2099 nm. The WG propagation losses were about 0.4 dB/cm. Regarding crystalline Ho WGs, Ho:YAG has been typically employed. In [10], a fs-DLW Ho:YAG WG laser pumped by a Tm fiber laser generated 1.88 W at 2090 nm with η = 29%. Recently, Q-switched mode-locking of a fs-DLW Ho:YAG WG laser has been realized resulting in 4.6 ps pulses at a repetition rate of 5.9 GHz [11].

There are no reports on fs-DLW Ho WGs based on anisotropic crystals. Among those, monoclinic (space group C_{2h} - C2/c) double tungstates (MDTs) with chemical formula KRE(WO₄)₂, where RE stands for Gd, Lu or Y are excellent hosts for Ho³⁺ doping [12]. They feature high Ho³⁺ doping levels, intense spectral bands distinguished

for different light polarizations, and weak concentration quenching of the fluorescence [13]. Efficient Ho MDT lasers have been demonstrated in bulk and thin-disk geometries [7,14]. As for the Ho MDT WGs, the only report is about a Tm,Ho:KY(WO₄)₂ planar WG laser that yielded 1.9 mW at 2051 nm with $\eta = 10.5\%$ [15].

The aim of the present paper is the demonstration of the first holmium WG laser based on a MDT crystal fabricated by fs-DLW. To date, various studies regarding fs-DLW WG lasers in MDTs doped with other rare-earth ions have been reported. The first one focused on type II WG lasers based on Yb³⁺-doped KGd(WO₄)₂ and KY(WO₄)₂ [16]. The preservation of the fluorescence and the Raman gain from a fs-DLW Nd:KGd(WO₄)₂ WG has been observed in [17]. Raman gain in fs-DLW WGs based on undoped KGd(WO₄)₂ was also reported [18]. Recently, efficient laser operation in channel WGs inscribed in Tm³⁺-doped KLu(WO₄)₂ was reported [19,20]. Different WG geometries (surface and buried WGs) were explored.

In the present work we used a 5 at% Ho:KGd(WO₄)₂ crystal (shortly Ho:KGdW) for the fs-DLW fabrication. It was grown by the Top-Seeded Solution Growth (TSSG) Slow-Cooling method using K₂W₂O₇ as a solvent [13]. The Ho³⁺ doping concentration N_{Ho} was $2.68 \times 10^{20} \text{ cm}^{-3}$, as determined by Electron Probe Micro-Analysis (EPMA). The fs-DLW was performed using 120 fs, 795 nm pulses from a Ti:Sapphire regenerative amplifier and a 40 \times microscope objective (NA = 0.65). The incident pulse energy was attenuated to 74 nJ at the sample surface and the crystal scanning speed was 400 $\mu\text{m/s}$. The polarization of the fs laser corresponded to $\mathbf{E} \parallel N_m$ in the crystal. The WG axis was along the N_g optical indicatrix axis of the biaxial KGdW. The WG was written through the entire sample length ($l = 5.5 \text{ mm}$). The end-facets were polished to laser-grade quality and remained uncoated.

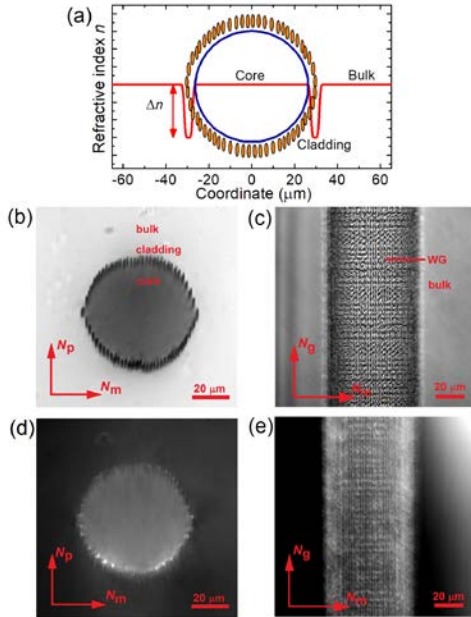


Fig. 1. (a) Schematic picture of the fs-DLW depressed index cladding WG (end-facet view). Red line - the refractive index (n) profile; (b-e) Transmission-mode confocal microscope pictures of the fs-DLW 5 at% Ho:KGdW WG: (b,d) end-facet view, (c,e) top view. (b,c) polarized light, (b) $P \parallel N_p$, (c) $P \parallel N_g$, $\lambda = 405 \text{ nm}$, (d,e) with crossed polarizer (P) and analyzer (A), (d) $P \parallel N_p$, $A \parallel N_m$, (e) $P \parallel N_g$, $A \parallel N_m$, $\lambda = 488 \text{ nm}$.

The fabricated micro-structure corresponds to a tubular depressed index cladding WG (type III), where photons from the propagating mode inside the cladding can tunnel out of the cladding, Fig. 1(a). In this case, the transverse thickness of the cladding and the magnitude of the negative refractive index change in the cladding ($\Delta n \approx -6 \times 10^{-4}$) are the key parameters that allow to control the WG "leaky mode" [21] propagation losses. During fs-DLW in MDTs, we have found that it is not easy to further increase the magnitude of the index depression in the cladding due to excessive damage of the crystal structure, which can entail bond breaking and cracking. Thus, the thickness of the cladding must be as large as possible to diminish the radiation losses. The upper limit for the in-depth cladding thickness is set by optical aberrations in the birefringent MDT crystals. For this reason, we have found the current cladding size to be effective for laser experiments.

The WG was characterized by confocal laser microscopy, Fig. 1(b-e). First, the polished end-facet was imaged using polarized light, Fig. 1(b). The WG consisted of a circular cladding (with a diameter of 60 μm) formed by individual damage tracks surrounding the inner core. The vertical and lateral sizes of the tracks were ~ 8 and 1.5 μm , respectively. The lateral track separation was $\sim 2 \mu\text{m}$. The WG central axis was located at 75 μm beneath the crystal surface. No cracks were observed in the WG core region with the selected parameters. When observing the top-surface of the WG, Fig. 1(c), a net-like barrel-shaped cladding was revealed. The damage tracks were continuous through the whole sample. The observation of the WG between crossed polarizers set along the optical indicatrix axes revealed a bright cladding, Fig. 1(d,e), attributed to the birefringence due to the stress-optic effect [22].

The structure modification in the cladding was confirmed by μ -Raman spectroscopy. The $\nu(\text{WOOW})^*\nu(\text{W-O})/\nu_3$ Raman mode of KGdW (centered at $\sim 685 \text{ cm}^{-1}$) related to the double oxygen bridge stretching vibrations which are characteristic for the MDT structure was analyzed. The intensity of the Raman peak, Fig. 2(a), and peak frequency, Fig. 2(b), were recorded to produce 2D maps. The reduced intensity and the blue-shift of the peak indicated a compromised crystalline order in the cladding. An anisotropic stress field extending beyond the WG cladding [22] is also revealed in Fig. 2(b).

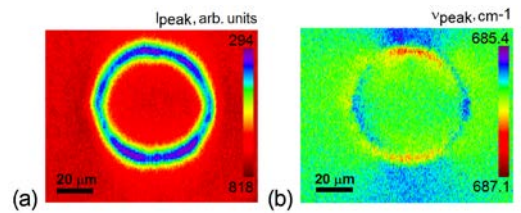


Fig. 2. μ -Raman mapping of the polished end-facet of the fs-DLW 5 at% Ho:KGdW WG, $g(mm)g$ geometry (Porto's notations), monitoring the $\sim 685 \text{ cm}^{-1}$ Raman peak: (a) Raman peak intensity, (b) peak position, $\lambda_{\text{exc}} = 514 \text{ nm}$.

The effect of fs-DLW on the properties of Ho³⁺ ions was studied by μ -luminescence spectroscopy, Fig. 3. The green $^5S_2 + ^5F_4 \rightarrow ^5I_7$ Ho³⁺ emission was analyzed in terms of luminescence intensity and wavelength shift, see Fig. 3(a,b). A reduction of the intensity and a wavelength red-shift for the Ho³⁺ luminescence in the cladding indicate the alteration of the crystal-field due to a reduced crystallinity. Contrary, in the WG core, the emission properties of Ho³⁺ remained unchanged with respect to the bulk crystal, Fig. 3(c).

Spectroscopic data for the $^5I_7 \leftrightarrow ^5I_8$ Ho³⁺ transition in KGdW, as shown in Fig. 3(d), are presented in Fig. 4 for light polarization $\mathbf{E} \parallel N_m$. The maximum absorption cross-section σ_{abs} is $2.0 \times 10^{-20} \text{ cm}^2$ at 1961 nm and the stimulated-emission (SE) cross-section, σ_{SE} , reaches

$2.7 \times 10^{-20} \text{ cm}^2$ at 2054 nm, Fig. 4(a). As Ho^{3+} ions exhibit reabsorption at the laser wavelengths, we also plot the gain cross-sections, $\sigma_{\text{gain}} = \beta\sigma_{\text{SE}} - (1 - \beta)\sigma_{\text{abs}}$, Fig. 4(b). Depending on the inversion ratio, $\beta = N_2(^5I_7)/N_{\text{Ho}}$, laser operation is expected around the local peaks at 2070 nm (for $\beta < 0.3$) and 2054 nm (for higher inversion). The measured luminescence decay lifetime $\tau_{\text{lum}}(^5I_7)$ from the WG core is 5.65 ms.

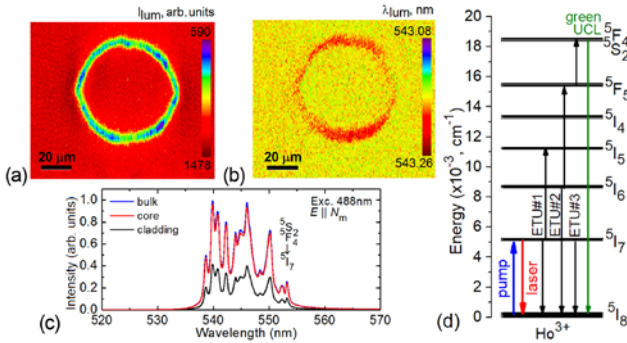


Fig. 3. (a-c) μ -luminescence mapping of the polished end-facet of the fs-DLW 5 at % Ho:KGdW WG for the $^5S_2 + ^5F_4 \rightarrow ^5I_7$ Ho^{3+} transition: (a) luminescence intensity, (b) peak wavelength, (c) spectra measured from the bulk, WG core and WG cladding, $\lambda_{\text{exc}} = 488 \text{ nm}$, excitation and detection are for light polarization $\mathbf{E} \parallel N_m$; (d) scheme of energy levels of Ho^{3+} in KGdW showing pump and laser transitions, ETU - energy-transfer upconversion, UCL - upconversion luminescence.

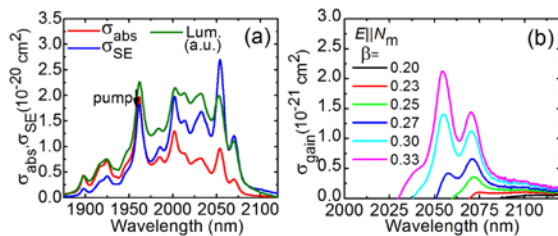


Fig. 4. Spectroscopy of the $^5I_7 \leftrightarrow ^5I_8$ transition of Ho^{3+} in KGdW: (a) absorption, σ_{abs} , and stimulated-emission (SE), σ_{SE} , cross-sections, green curve - luminescence spectrum from the core of the fs-DLW WG; (b) gain cross-sections, $\sigma_{\text{gain}} = \beta\sigma_{\text{SE}} - (1 - \beta)\sigma_{\text{abs}}$, for different inversion rates $\beta = N_2(^5I_7)/N_{\text{Ho}}$. The light polarization is $\mathbf{E} \parallel N_m$.

The laser set-up is shown in Fig. 5(a). The Ho WG was pumped by an in-house CW diode-pumped Tm:KLu(WO₄)₂ microchip laser [23] delivering $\sim 3 \text{ W}$ at 1960 nm ($M^2 \approx 1$). The polarization of the pump corresponded to $\mathbf{E} \parallel N_m$ in the Ho:KGdW crystal. The pump light was coupled into the WG using a pair of spherical lenses (focal lengths: $f = 150$ and 60 mm for collimation and focusing, respectively). The pump coupling efficiency was estimated from the geometrical overlap of the pump beam and the WG core, $\eta_{\text{coupl}} = 70 \pm 1\%$ (including the Fresnel losses). The Ho:KGdW sample was placed on a passively-cooled Al support. The laser cavity was made of a flat pump mirror (PM) coated for high transmission ($T > 94\%$) at 1900-2000 nm and high reflection (HR) at 2020-2150 nm, and flat output couplers (OCs) with transmission $T_{\text{OC}} = 1.5\% \dots 30\%$ at 1800-2100 nm. Both the PM and the OC were placed as close as possible to the WG end-faces with minimum air gaps. No index-matching liquid was used. The single-pass pump absorption was determined from the pump-transmission experiment at the threshold pump power. Due to the back-reflection of

the OCs at the pump wavelength ($R > 70\%$), some of the non-absorbed pump power was coupled back in the WG and thus improved the pump absorption η_{abs} . The total η_{abs} value was calculated accounting for the back-reflection of the pump as $40\text{--}44 \pm 1\%$ depending on the OC. It was also confirmed using a rate equation modelling accounting for the ground-state bleaching. A photograph of the pumped WG is shown in Fig. 5(b).

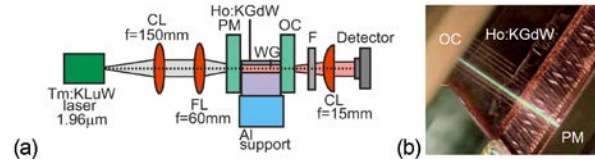


Fig. 5. (a) Scheme of the in-band pumped fs-DLW 5 at % Ho:KGdW WG laser: CL and FL - collimating and focusing lenses, respectively, PM - pump mirror, OC - output coupler, F - long-pass filter; (b) photograph of the pumped WG.

The input-output dependences for the fs-DLW Ho WG laser are shown in Fig. 6(a). The laser output was linearly polarized, $\mathbf{E} \parallel N_m$, the polarization was naturally selected by the anisotropy of the gain. For the output coupler with $T_{\text{OC}} = 30\%$, the laser generated a maximum output power of 212 mW at 2055 nm with a slope efficiency η of 67.2% with respect to the absorbed pump power P_{abs} , Fig. 6(a). The laser threshold was at $P_{\text{abs}} = 180 \text{ mW}$ and the optical-to-optical efficiency vs. the incident pump power $\eta_{\text{opt}} = 12.1\%$. For lower T_{OC} , the laser performance gradually deteriorated. The output dependences were linear indicating weak thermal effects even considering the passive cooling of the WG. No crystal damage was observed.

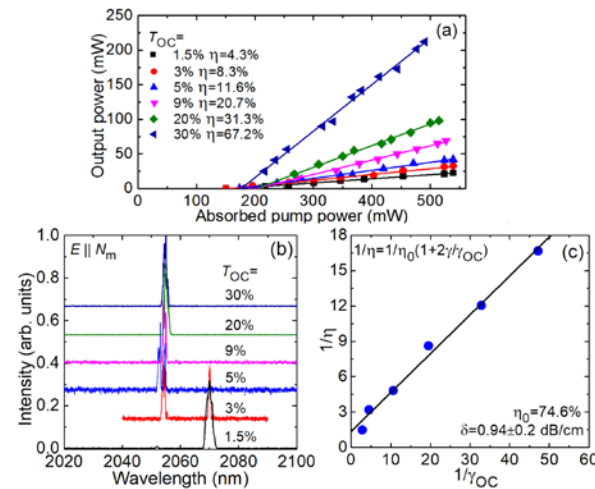


Fig. 6. In-band pumped fs-DLW 5 at % Ho:KGdW WG laser: (a) input-output dependences, η - slope efficiency; (b) typical laser emission spectra measured at the maximum P_{abs} ; (c) evaluation of the losses (Caird analysis). The laser polarization is $\mathbf{E} \parallel N_m$.

Typical laser emission spectra measured at maximum P_{abs} are shown in Fig. 6(b). The WG laser emitted at $\sim 2055 \text{ nm}$ for $T_{\text{OC}} \geq 3\%$ and at $\sim 2070 \text{ nm}$ for lower output coupling. This spectral behavior is well in line with the gain spectra, Fig. 4(b).

The propagation (passive) loss of the WG was estimated using the Caird analysis modified for high output coupling [24], $1/\eta = (1/\eta_0)(1 + 2\gamma/\gamma_{\text{oc}})$, where $\gamma = -\ln(1 - L)$, L is an internal loss per pass, $\gamma_{\text{oc}} = -\ln(1$

– T_{OC}), and η_0 is an intrinsic slope efficiency. From the linear fit shown in Fig 6(c), the values of $\eta_0 = 74.6\%$ and the propagation loss $\delta = 4.34L/l = 0.94 \pm 0.2$ dB/cm were determined. The measured near-field mode profile of the output beam from the fs-DLW Ho:KGdW laser is shown in Fig. 8. It is spatially multimode. Considering a step-index model of the circular-cladding WG (similar to fibers), for single-mode operation, the normalized frequency $V = 2\pi a \cdot \text{N.A.} / \lambda_L < 2.405$ (a – radius of the WG core, $\text{N.A.} \approx 2n \cdot \Delta n$ – numerical aperture of the WG, $n = 1.97$ for $E \parallel N_m$, λ_L – laser wavelength). This gives an estimation for the core diameter of the single-mode WG: $2a < 32 \mu\text{m}$.

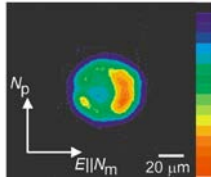


Fig. 8. Spatial profile of the laser mode from the fs-DLW 5 at% Ho:KGdW WG laser (near-field, $T_{OC} = 30\%$, $P_{abs} = 0.44$ W).

Table 1. Output Characteristics of Fs-DLW Holmium Waveguide Lasers Reported So Far.

Material	P*	λ_p , μm	P_{out} , W	λ_L , nm	η , %	Ref.
Ho:Tm:ZBLAN	TiSa	0.790	0.076	2052	20 ^{Abs}	[8]
Ho:YAG	TFL	1.908	1.88	2090	29 ^{Inc}	[10]
Ho:Yb:YAG	TFL	1.908	0.33	2090	9 ^{Inc}	[10]
Ho:ZBLAN	TFL	1.945	1.09	2070	50.9 ^{Inc}	[9]
Ho:ZBLAN	LD	1.150	0.026	2900	19.5 ^{Abs}	[25]
Ho:KGdW	TL	1.946	0.212	2055	67.2^{Abs}	**

*Pump: TiSa – Ti:Sapphire laser; TFL – thulium fiber laser; LD – laser diode; TL – thulium laser (bulk); **This work.

To conclude, we report on the first fs-DLW holmium waveguide laser based on an anisotropic (low-symmetry) crystalline material. A 5 at% Ho:KGd(WO₄)₂ MDT crystal was used to fabricate a buried circular cladding WG with 60 μm core diameter. In the CW operation mode, the in-band pumped Ho WG laser generated >200 mW at 2055 nm with a record slope efficiency of 67.2%, cf. Table 1 (whilst the laser output was spatially multimode). The WG propagation losses were reasonably low, <1 dB/cm. Further power scaling to multi-watt output seems feasible by applying powerful pump sources (e.g., Tm fiber lasers) and optimizing the Ho³⁺ doping concentration (3-10 at%). For this, more attention has to be paid for eliminating the thermal effects, at least, by applying an active cooling of the WG. The reduction of the WG diameter to less than 40 μm is expected to provide single-transverse-mode operation. Such single-mode Ho WGs will serve as an absis for development of GHz-repetition-rate WG mode-locked oscillators. Further work is planned to achieve single-transverse-mode operation.

Funding. Spanish Government (MAT2016-75716-C2-1-R (AEI/FEDER/UE), TEC 2014-55948-R, FIS2017-87970-R); Junta de Castilla y León (UIC016, SA287P18); Generalitat de Catalunya (2017SGR755). European Union’s Horizon 2020 research and innovation program under the Marie Skłodowska-Curie Individual Fellowship (grant No. 747055).

Acknowledgments. E. K. acknowledges financial support from the Generalitat de Catalunya under grants 2016FI_B00844, 2017FI_B100158 and 2018FI_B200123. F. D. acknowledges additional

support through the ICREA academia award 2010ICREA-02 for excellence in research. A. R. acknowledges funding from the European Union’s Horizon 2020 research and innovation programme under the Marie Skłodowska-Curie Individual Fellowship Grant Agreement No. 747055. P. L. acknowledges financial support from the Government of the Russian Federation (Grant 074-U01) through ITMO Post-Doctoral Fellowship scheme. The research leading to these results has received funding from the European Community’s Horizon 2020 research and innovation programme under grant agreement n° 654148 (Laserlab-EUROPE. Project No. MBI MBI002365).

References

1. R. Osellame, G. Cerullo, and R. Ramponi, “Femtosecond Laser Micromachining: Photonic and Microfluidic Devices in Transparent Materials” (Springer, 2012).
2. F. Chen, and J. R. V. Aldana, *Laser Photon. Rev.* **8**, 251 (2014).
3. A. G. Okhrimchuk, A. V. Shestakov, I. Khrushchev, and J. Mitchell, *Opt. Lett.* **30**, 2248 (2005).
4. A. Ródenas, G. A. Torchia, G. Lífante, E. Cantelar, J. Lamela, F. Jaque, L. Roso, and D. Jaque, *Appl. Phys. B* **95**, 85 (2009).
5. Y. Tan, A. Rodenas, F. Chen, R. R. Thomson, A. K. Kar, D. Jaque, and Q. Lu, *Opt. Express* **18**, 24994 (2010).
6. Y. Ren, G. Brown, A. Ródenas, S. Beecher, F. Chen, and A. K. Kar, *Opt. Lett.* **37**, 3339 (2012).
7. P. Loiko, J. M. Serres, X. Mateos, K. Yumashev, N. Kuleshov, V. Petrov, U. Griebner, M. Aguiló, and F. Díaz, *Opt. Lett.* **40**, 344 (2015).
8. D. G. Lancaster, S. Gross, H. Ebendorff-Heidepriem, A. Fuerbach, M. J. Withford, and T. M. Monro, *Opt. Lett.* **37**, 996 (2012).
9. D. G. Lancaster, V. J. Stevens, V. Michaud-Belleau, S. Gross, A. Fuerbach, and T. M. Monro, *Opt. Express* **23**, 32664 (2015).
10. S. McDaniel, F. Thorburn, A. Lancaster, R. Stites, G. Cook, and A. Kar, *Appl. Opt.* **56**, 3251 (2017).
11. F. Thorburn, A. Lancaster, S. A. McDaniel, G. Cook, and A. K. Kar, in *Conference on Lasers and Electro-Optics* (Optical Society of America, 2017), p. SM11.5.
12. V. Jambunathan, X. Mateos, M. C. Pujol, J. J. Carvajal, F. Díaz, M. Aguiló, U. Griebner, and V. Petrov, *Opt. Express* **19**, 25279 (2011).
13. V. Jambunathan, X. Mateos, P. A. Loiko, J. M. Serres, U. Griebner, V. Petrov, K. V. Yumashev, M. Aguiló, and F. Díaz, *J. Lumin.* **179**, 50 (2016).
14. X. Mateos, S. Lamrini, K. Scholle, P. Fuhrberg, S. Vatik, P. Loiko, I. Vedin, M. Aguiló, F. Díaz, U. Griebner, and V. Petrov, *Opt. Lett.* **42**, 3490 (2017).
15. C. V. R. Madroñero, X. Mateos, P. Loiko, K. Yumashev, V. Petrov, U. Griebner, M. Aguiló, and F. Díaz, *Laser Phys. Lett.* **13**, 095801 (2016).
16. F. M. Bain, A. A. Lagatsky, R. R. Thomson, N. D. Psaila, N. V. Kuleshov, A. K. Kar, W. Sibbett, and C. T. A. Brown, *Opt. Express* **17**, 22417 (2009).
17. X. Liu, S. Qu, Y. Tan, and F. Chen, *Appl. Opt.* **50**, 930 (2011).
18. S. M. Eaton, C. A. Merchant, R. Iyer, A. J. Zilkie, A. S. Helmy, J. S. Aitchison, P. R. Herman, D. Kraemer, R. J. D. Miller, C. Hnatovsky, and R. S. Taylor, *Appl. Phys. Lett.* **92**, 081105 (2008).
19. E. Kifle, X. Mateos, J. R. V. de Aldana, A. Ródenas, P. Loiko, S. Y. Choi, F. Rotermund, U. Griebner, V. Petrov, M. Aguiló, and F. Díaz, *Opt. Lett.* **42**, 1169 (2017).
20. E. Kifle, P. Loiko, J. R. Vázquez de Aldana, C. Romero, A. Ródenas, S. Y. Choi, J. E. Bae, F. Rotermund, V. Zakharov, A. Veniaminov, M. Aguiló, F. Díaz, U. Griebner, V. Petrov, and X. Mateos, *Photon. Res.* **6**, 971 (2018).
21. H. Karakuzu, M. Dubov, and S. Boscolo, *Opt. Express* **21**, 17122 (2013).
22. H.-D. Nguyen, A. Ródenas, J. R. Vázquez de Aldana, J. Martínez, F. Chen, M. Aguiló, M. C. Pujol, and F. Díaz, *Opt. Express* **24**, 7777 (2016).
23. J. M. Serres, X. Mateos, P. Loiko, K. Yumashev, N. Kuleshov, V. Petrov, U. Griebner, M. Aguiló, and F. Díaz, *Opt. Lett.* **39**, 4247 (2014).
24. J. Morris, N. K. Stevenson, H. T. Bookey, A. K. Kar, C. T. A. Brown, J. M. Hopkins, M. D. Dawson, and A. A. Lagatsky, *Opt. Express* **25**, 14910 (2017).

25. D. G. Lancaster, S. Gross, H. Ebendorff-Heidepriem, M. J. Withford, T. M. Monro, and S. D. Jackson, *Opt. Lett.* **38**, 2588 (2013).